

# Interface-Enhanced Spin-Orbit Torques and Current-Induced Magnetization Switching of Pd/Co/AIO<sub>x</sub> Layers

Abhijit Ghosh, Kevin Garello, Can Onur Avci, Mihai Gabureac, and Pietro Gambardella

*Department of Materials, ETH Zürich, Hönggerberggring 64, CH-8093 Zürich, Switzerland*

(Received 25 July 2016; revised manuscript received 29 October 2016; published 6 January 2017)

Magnetic heterostructures that combine large spin-orbit torque efficiency, perpendicular magnetic anisotropy, and low resistivity are key to developing electrically controlled memory and logic devices. Here, we report on vector measurements of the current-induced spin-orbit torques and magnetization switching in perpendicularly magnetized Pd/Co/AIO<sub>x</sub> layers as a function of Pd thickness. We find sizable dampinglike (DL) and fieldlike (FL) torques, on the order of 1 mT per  $10^7$  A/cm<sup>2</sup>, which have different thicknesses and magnetization angle dependencies. The analysis of the DL torque efficiency per unit current density and the electric field using drift-diffusion theory leads to an effective spin Hall angle and spin-diffusion length of Pd larger than 0.03 and 7 nm, respectively. The FL spin-orbit torque includes a significant interface contribution, is larger than estimated using drift-diffusion parameters, and, furthermore, is strongly enhanced upon rotation of the magnetization from the out-of-plane to the in-plane direction. Finally, taking advantage of the large spin-orbit torques in this system, we demonstrate bipolar magnetization switching of Pd/Co/AIO<sub>x</sub> layers with a similar current density to that used for Pt/Co layers with a comparable perpendicular magnetic anisotropy.

DOI: 10.1103/PhysRevApplied.7.014004

## I. INTRODUCTION

Spin-orbit torques (SOTs) generated by current injection in normal-metal/ferromagnet (NM/FM) bilayers have attracted considerable attention as a method to induce magnetization switching of thin FM films and magnetic tunnel-junction devices [1–7]. Although the bulk or interface origin of the spin current giving rise to the dampinglike (DL) and fieldlike (FL) SOT components is a matter of debate [8–11], it has been established that the strongest SOTs are found in NMs with large spin-orbit coupling, and hence a large spin Hall effect (SHE) and a small spin-diffusion length ( $\lambda$ ), such as the *5d* metals Pt, W, and Ta [12–19]. For this reason, the *4d* metals have been largely cast aside in the quest for large SOTs, even though several studies of the SHE in these materials show sizable spin Hall angles, of the order of  $\gamma_{\text{SH}} \sim 0.01$  [20–24].

Pd-based heterostructures constitute an apparent exception to this trend: recent studies of [Pd/Co]<sub>N</sub> multilayers [25] and Pd/FePd/MgO trilayers [26] evidenced DL and FL effective fields of the same order of magnitude or larger than those found in Pt- and Ta-based structures, reaching up to more than 10 mT for an injected current density of  $j = 10^7$  A/cm<sup>2</sup>. The effective spin Hall angle required to model the SOTs according to spin-diffusion theory is  $\gamma_{\text{SH}} > 1$  in [Pd/Co]<sub>N</sub> [25] and  $\gamma_{\text{SH}} \approx 0.15$  in Pd/FePd/MgO [26], which is substantially larger than previous estimates of  $\gamma_{\text{SH}}$  in Pd [20–24]. This comparison calls for further investigations of the SOTs resulting from Pd as well as of the possibility of using Pd to induce magnetization switching, which has not been reported to date.

In this work, we present a study of current-induced SOTs and magnetization switching in Pd/Co/AIO<sub>x</sub> trilayers with

varying Pd thicknesses. We focus on the simple trilayer structure to avoid the complexity resulting from multiple interfaces and current paths in [Pd/Co]<sub>N</sub> multilayers, which complicate the analysis and interpretation of the experimental data [25]. Our study is based on the harmonic Hall voltage method to measure SOT [14–16,27,28] and includes a detailed magnetotransport characterization as well as the analysis of magnetothermal contributions to the Hall resistance [14,29]. We report strong DL and FL SOT amplitudes and efficient magnetization switching for this system, combined with large perpendicular magnetic anisotropy (PMA) and relatively low resistivity. We further observe a distinct thickness dependence of the DL and FL torques and discuss different models to account for the SOT efficiency. The main results are summarized at the end of this paper.

## II. EXPERIMENT

Our samples are Ta(0.8 nm)/Pd( $t_{\text{Pd}}$ )/Co(0.6 nm)/AIO<sub>x</sub>(1.6 nm) layers grown on thermally oxidized Si substrates by dc magnetron sputtering in an Ar pressure of  $2 \times 10^{-3}$  Torr. The Al cap layer is oxidized for 37 s under a partial O<sub>2</sub> pressure of  $7 \times 10^{-3}$  Torr in order to increase the PMA of Co/Pd. The Ta seed layer is used to improve the uniformity of Pd; because of its high resistivity and reduced thickness, such a layer plays a negligible role in the generation of SOTs, as we confirm by measuring Pd/Co/AIO<sub>x</sub> structures grown with a Ti seed. The rms roughness measured by atomic-force microscopy is found to vary between 0.15 nm ( $t_{\text{Pd}} = 1.5$  nm) and 0.13 nm ( $t_{\text{Pd}} = 8$  nm). The as-grown layers are patterned using UV

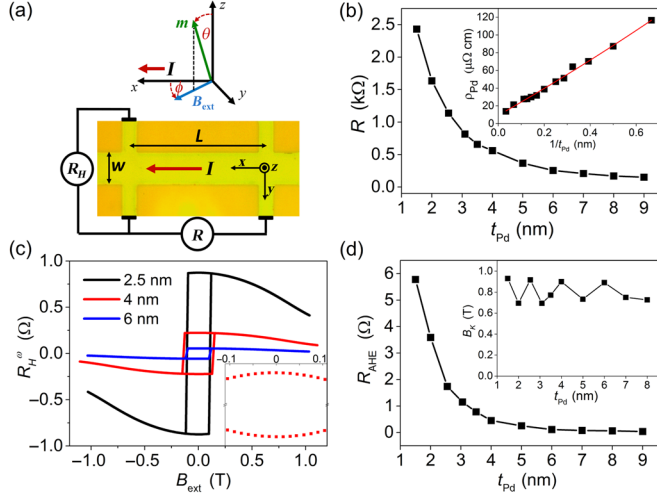


FIG. 1. (a) Schematic of the experimental geometry and scanning electron micrograph of a Pd/Co/AIO<sub>x</sub> Hall bar. (b) Resistance as a function of Pd thickness. (Inset) Pd resistivity as a function of inverse thickness. The solid line is a linear fit. (c) First harmonic Hall resistance  $R_H^\omega$  of three representative samples as a function of an external field applied at  $\theta_B = 84^\circ$  and  $\phi = 0^\circ$ . (Inset) Detail of the low-field region of the 4-nm sample. (d)  $R_{\text{AHE}}$  as a function of Pd thickness. (Inset) Anisotropy field  $B_K$ .

lithography and dry etching into Hall bars with a width  $w = 10 \mu\text{m}$  and a length  $L = 50 \mu\text{m}$ , as shown in Fig. 1(a).

For the magnetotransport characterization, the samples are mounted in the gap of an electromagnet producing a field  $B_{\text{ext}}$  and allowing for rotating the current direction relative to the magnetization ( $\mathbf{m}$ ). The experiments are performed at room temperature using an ac current  $I = I_0 \sin(\omega t)$  with an amplitude  $I_0$  and a frequency  $\omega/2\pi = 10$  Hz.  $I_0$  ranges between 3 and 14 mA in samples with  $t_{\text{Pd}} = 1.5$  and 9 nm, respectively, and is adjusted in order to keep the current density flowing through Pd between  $j_{\text{Pd}} = 1 \times 10^7$  and  $1.5 \times 10^7$  A/cm<sup>2</sup>. The harmonic Hall-voltage measurements are performed by taking the Fourier transform of the ac Hall resistance recorded for 10 s at each value of the applied field and current. The first harmonic Hall resistance is analogous to a dc Hall measurement and is given by

$$R_H^\omega = R_{\text{AHE}} \cos \theta + R_{\text{PHE}} \sin^2 \theta \sin(2\phi), \quad (1)$$

where  $R_{\text{AHE}}$  and  $R_{\text{PHE}}$  are the anomalous and planar Hall coefficients, and  $\theta$  and  $\phi$  represent the polar and azimuthal angles of the magnetization, respectively.

Current-induced effects are characterized by measuring the second harmonic Hall resistance,  $R_H^{2\omega}$ , which arises from the mixing of the ac current with the Hall effect modulated by the oscillations of the magnetization induced by the DL and FL torques [14–16,27,28]. This term accounts for the SOT effective fields, which are proportional to  $I$ , as well as for magnetothermal effects that are proportional to  $I^2$  [14,16,29]. Following Ref. [29], we have

$$R_H^{2\omega} = [R_{\text{AHE}} - 2R_{\text{PHE}} \cos \theta \sin(2\phi)] \frac{d \cos \theta}{dB_{\text{ext}}} \frac{B_\theta^I}{\sin(\theta_B - \theta)} + R_{\text{PHE}} \sin^2 \theta \frac{2 \cos(2\phi)}{B_{\text{ext}} \sin \theta_B} B_\phi^I + R_{\nabla T}^{2\omega}, \quad (2)$$

where  $B_\theta^I$  and  $B_\phi^I$  are the polar and azimuthal components of the current-induced effective fields, respectively, including both SOT and the Oersted field, and  $R_{\nabla T}^{2\omega} \propto (\nabla T \times \mathbf{m}) \cdot \mathbf{y}$  is the thermal Hall resistance associated with the anomalous Nernst effect. The latter is caused by the unintentional out-of-plane and in-plane temperature gradients  $\nabla T$  produced through Joule heating and asymmetric heat dissipation in the trilayer [29].

To separate the SOT contributions from  $R_{\nabla T}^{2\omega}$ , we exploit the different behaviors of  $B_\theta^I$  and  $R_{\nabla T}^{2\omega}$  as a function of  $B_{\text{ext}}$ , as explained in detail in Ref. [29] and the Supplemental Material [30]. Finally, in order to explicitly show the relationship between  $B_\theta^I$  and  $B_\phi^I$  in Eq. (2) and the DL and FL SOT effective fields, we express the latter in spherical coordinates [14]:

$$\mathbf{B}^{\text{DL}} = B_\theta^{\text{DL}} \cos \phi \mathbf{e}_\theta - B_\phi^{\text{DL}} \cos \theta \sin \phi \mathbf{e}_\phi, \quad (3)$$

$$\mathbf{B}^{\text{FL}} = -B_\theta^{\text{FL}} \cos \theta \sin \phi \mathbf{e}_\theta - B_\phi^{\text{FL}} \cos \phi \mathbf{e}_\phi, \quad (4)$$

where the coefficients  $B_\theta^{\text{DL}}$ ,  $B_\theta^{\text{FL}}$ ,  $B_\phi^{\text{DL}}$ , and  $B_\phi^{\text{FL}}$  represent the polar and azimuthal amplitudes of the DL and FL SOTs. In the ‘‘isotropic torque’’ limit usually considered in the SOT literature, Eqs. (3) and (4) are obtained by projecting  $\mathbf{B}^{\text{DL}} = B_0^{\text{DL}}(\mathbf{m} \times \mathbf{y})$  and  $\mathbf{B}^{\text{FL}} = B_0^{\text{FL}}[\mathbf{m} \times (\mathbf{m} \times \mathbf{y})]$  onto the unit vectors  $\mathbf{e}_\theta$  and  $\mathbf{e}_\phi$  and by assuming  $B_{\theta,\phi}^{\text{DL}} = B_0^{\text{DL}}$  and  $B_{\theta,\phi}^{\text{FL}} = B_0^{\text{FL}}$ .

General models and SOT vector measurements, however, have shown that  $B_{\theta,\phi}^{\text{DL}}$  and  $B_{\theta,\phi}^{\text{FL}}$  can be functions of the magnetization orientation [14,31,32]. In such a case, as in the present work, the four unknown coefficients in Eqs. (3) and (4) must be determined by four independent measurements of  $R_H^{2\omega}$  as a function of  $B_{\text{ext}}$ , applied in plane along  $\phi = 0^\circ, \pm 45^\circ$ , and  $90^\circ$ . All of the SOT values reported in this work are normalized to  $j_{\text{Pd}} = 1 \times 10^7$  A/cm<sup>2</sup> for ease of comparison with data in the literature.

### III. RESULTS

#### A. Resistivity and magnetic anisotropy

Figure 1(b) shows the resistance of the Pd/Co/AIO<sub>x</sub> layers as a function of Pd thickness. Using a simple parallel-resistor model and assuming that the conductivity of Co remains constant across the series, we find that the resistivity of Pd varies approximately as  $\rho_{\text{Pd}} \propto 1/t_{\text{Pd}}$  [inset of Fig. 1(b)]. This result is in line with previous investigations of the resistivity of Pd thin films [33], which is similar to that of Pt [34] and significantly smaller than that

of  $\beta$ -W and  $\beta$ -Ta films. The Hall resistance  $R_H^\omega$  is shown in Fig. 1(c) as a function of  $B_{\text{ext}}$  applied at an angle  $\theta_B = 84^\circ$  relative to the sample normal. As is customary in SOT investigations of PMA materials, the external field is slightly tilted off plane in order to prevent the formation of magnetic domains. Accordingly, we observe that the magnetization loops are reversible as long as  $\mathbf{m}$  does not switch direction, as expected for a coherent rotation of the magnetization, and that  $R_H^\omega$  decreases with an increasing  $B_{\text{ext}}$  as  $\mathbf{m}$  tilts away from  $\mathbf{z}$ . When  $\phi = 0^\circ$  or  $90^\circ$ ,  $R_H^\omega$  is proportional to  $\mathbf{m} \cdot \mathbf{z}$ , which allows us to derive the angle  $\theta = \cos^{-1}(R_H^\omega/R_{\text{AHE}})$  as a function of the applied field. We observe also that the maximum amplitude of  $R_H^\omega$  decreases with an increasing Pd thickness owing to the decrease of the AHE resulting from current shunting through Pd [Fig. 1(d)]. Our data indicate that both the AHE and the PHE are roughly proportional to  $t_{\text{Pd}}^{-3}$  rather than to  $\rho_{\text{Pd}}/t_{\text{Pd}} \propto t_{\text{Pd}}^{-2}$ , as would be expected for a parallel-resistor model of the Co and Pd layers. This result suggests that the AHE and the magnetoresistance are enhanced at the Pd/Co interface relative to bulk Co, in agreement with studies of the AHE in  $[\text{Co}/\text{Pd}]_N$  multilayers [35].

The inset of Fig. 1(d) shows the effective magnetic anisotropy field calculated by using the macrospin approximation:  $B_K = B_{\text{ext}}(\sin \theta_B / \sin \theta - \cos \theta_B / \cos \theta)$ . We find that  $B_K$  varies between 0.7 and 0.9 T, with no systematic variation as a function of Pd thickness and independently of the in-plane direction of the magnetization. The corresponding uniaxial magnetic-anisotropy energy is thus  $K_u = B_K M_s / 2 + \mu_0 M_s^2 / 2 = (1.5 \pm 0.1) \times 10^6 \text{ J/m}^3$ , where  $M_s = 1.27 \times 10^6 \text{ A/m}$  is the saturation magnetization measured by a superconducting quantum interference device. Interestingly,  $K_u$  for Pd/Co/ $\text{AlO}_x$  is comparable or larger relative to  $[\text{Pd}/\text{Co}]_N$  multilayers [36–38], which we attribute to the top oxide layer favoring strong PMA through the formation of Co–O bonds [39,40].

## B. Spin-orbit torques

The SOT measurements are performed by analyzing the second harmonic Hall resistance that arises due to the mixing of the ac current with the ac oscillations of the magnetization induced by the DL and FL torques [Eq. (2)]. Because the DL torque is larger when  $\mathbf{m}$  is oriented in the  $x$ - $z$  plane, whereas the FL torque tends to align  $\mathbf{m}$  towards  $y$ , measurements taken at  $\phi = 0^\circ$  ( $\phi = 90^\circ$ ) mainly reflect the strength of the DL (FL) effective fields. Figures 2(a) and 2(b) show  $R_H^{2\omega}$  measured at  $\phi = 0^\circ$  and  $\phi = 90^\circ$  after the subtraction of  $R_{\text{VT}}^{2\omega}$  [30]. These curves are, respectively, odd and even with respect to magnetization reversal, reflecting the different symmetry of  $B^{\text{DL}}$  and  $B^{\text{FL}}$  [14]. Similarly to the  $R_H^\omega$  case, we observe that the amplitude of  $R_H^{2\omega}$  decreases with an increasing Pd thickness, which limits the signal-to-noise ratio and, consequently, the range of our SOT measurements to  $t_{\text{Pd}} \leq 8 \text{ nm}$ . Figures 2(c) and 2(d)

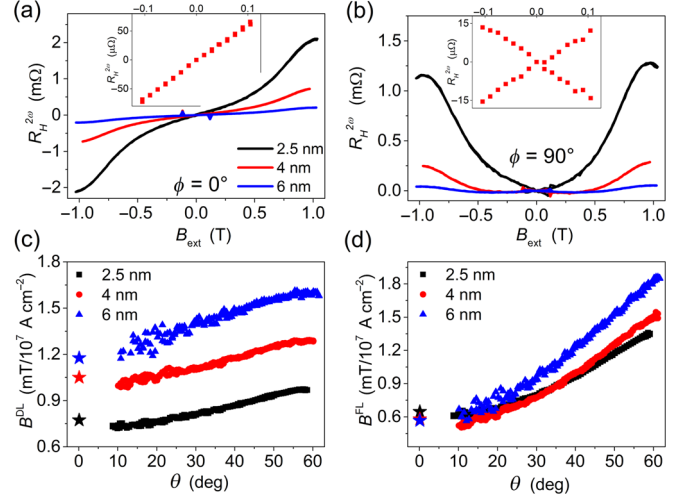


FIG. 2. Second harmonic Hall resistance  $R_H^{2\omega}$  as a function of applied field at (a)  $\phi = 0^\circ$  and (b)  $\phi = 90^\circ$ . (Insets)  $R_H^{2\omega}$  in the small-angle limit ( $\theta \leq 7^\circ$ ). (c)  $B^{\text{DL}}$  and (d)  $B^{\text{FL}}$  extracted from the data in (a) and (b), respectively, as a function of the polar magnetization angle  $\theta$ . The  $B^{\text{DL}}$  and the  $B^{\text{FL}}$  obtained using the small-angle approximation are indicated by a star.

show the effective fields  $B_\theta^{\text{DL}}$  and  $B_\theta^{\text{FL}}$  as a function of  $\theta$ , obtained by  $R_H^{2\omega}$  using Eqs. (2)–(4). We find that the DL and FL fields have the same sign as measured for Pt/Co/ $\text{AlO}_x$  [1,14,41] and increase as the magnetization rotates towards the plane of the layers. Compatibly with the uniaxial symmetry of the system, the angular dependence of the DL and FL fields can be modeled by a Fourier-series expansion of the type  $B_\theta^{\text{DL,FL}} = B_0^{\text{DL,FL}} + B_2^{\text{DL,FL}} \sin^2 \theta + B_4^{\text{DL,FL}} \sin^4 \theta + \dots$ , whereas the azimuthal components are only weakly angle dependent and are approximated by  $B_\phi^{\text{DL,FL}} \approx B_0^{\text{DL,FL}}$  [14]. The values of the zeroth-, second-, and fourth-order  $B_\theta^{\text{DL,FL}}$  coefficients are obtained by fitting the data in Figs. 2(c) and 2(d) according to this expansion. Additionally, we present data obtained using the small-angle approximation [28], which yields accurate values for  $B_0^{\text{DL,FL}}$  when  $\theta \approx 0^\circ$  [stars in Figs. 2(c) and 2(d)]. This approximation is valid as long as  $R_H^{2\omega}$  varies linearly with the applied field, as shown in the insets of Figs. 2(a) and 2(b), and is equivalent to Eq. (2) in this limit.

Figures 3(a)–3(c) report the isotropic and angle-dependent SOT amplitudes as a function of  $t_{\text{Pd}}$ , normalized to  $j_{\text{Pd}} = 10^7 \text{ A/cm}^2$ . To obtain the isotropic FL SOT component,  $B_0^{\text{FL}}$ , the Oersted field is calculated as  $B^{\text{Oe}} = \mu_0 j_{\text{Pd}} t_{\text{Pd}} / 2$  [open triangles in Fig. 3(a)] and subtracted from the total FL effective field derived from  $R_H^{2\omega}$  (open dots). The coefficients  $B_0^{\text{DL(FL)}}$ , shown in Fig. 3(a), represent the magnetic field induced by the DL (FL) torque when  $\mathbf{m} \parallel \mathbf{z}$ , whereas  $B_{2+4}^{\text{DL(FL)}}$ , shown in Fig. 3(b), represents the angle-dependent contributions, and  $B_{0+2+4}^{\text{DL(FL)}}$ , shown in Fig. 3(c), represents the total amplitude of the field when  $\mathbf{m} \parallel \mathbf{x}(\mathbf{y})$ .

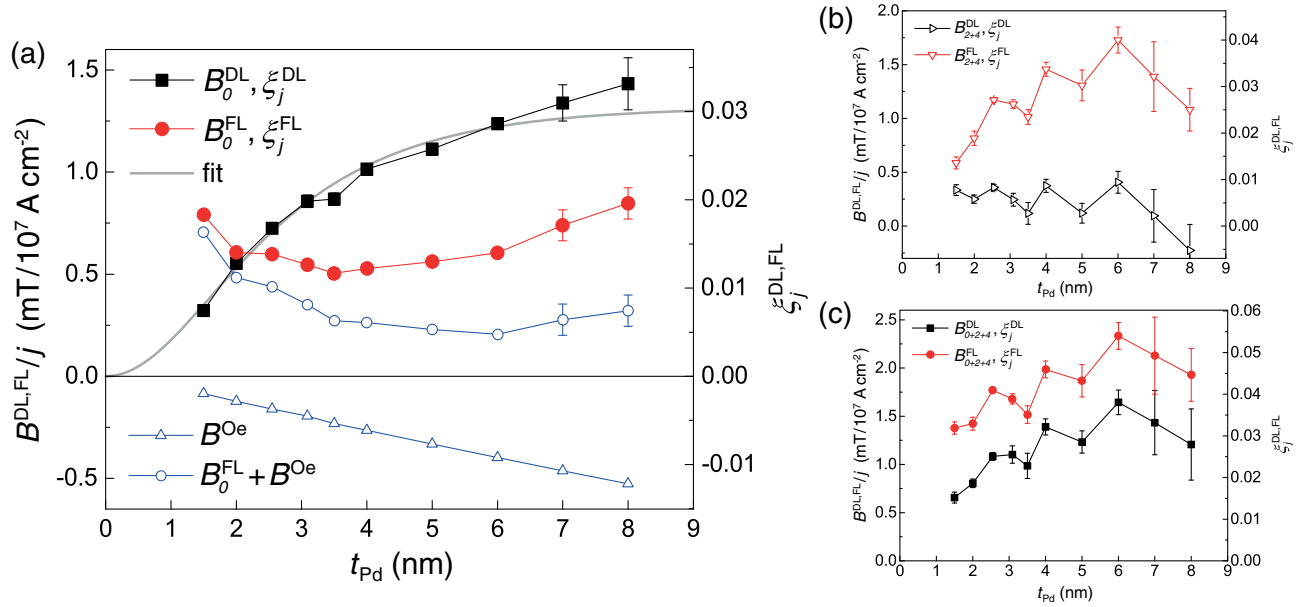


FIG. 3. SOT fields per unit current density as a function of  $t_{Pd}$ . (a) Isotropic amplitudes  $B_0^{DL}/j_{Pd}$  and  $B_0^{FL}/j_{Pd}$ , corresponding to perpendicular magnetization. (b) Angle-dependent amplitudes  $B_{2+4}^{DL}/j_{Pd}$  and  $B_{2+4}^{FL}/j_{Pd}$ . (c) Total amplitudes for in-plane magnetization,  $B_{0+2+4}^{DL}/j_{Pd}$  and  $B_{0+2+4}^{FL}/j_{Pd}$ . The SOT efficiency  $\xi_j^{DL(FL)}$  is shown on the right scale.

For comparison with literature data, we plot also the SOT efficiency (right scale), defined by

$$\xi_j^{DL(FL)} = \frac{2e}{\hbar} M_s t_{Co} \frac{B^{DL(FL)}}{j_{Pd}}, \quad (5)$$

which represents the ratio of the spin current absorbed by the FM to the charge current injected in the NM layer [12,42]. Remarkably, we find that the ratio  $B_0^{DL}/j_{Pd}$  increases with an increasing  $t_{Pd}$ , whereas  $B_0^{FL}/j_{Pd}$  has a nonmonotonic dependence on  $t_{Pd}$ . This finding is the first indication that the interface and bulk contributions to the two torques differ in magnitude. Moreover, we observe that the SOT efficiency depends on the orientation of the magnetization relative to the current direction. Specifically, the angular dependence of the FL SOT is much stronger than that of the DL SOT [Fig. 3(b)], such that the total FL torque is larger than the total DL torque when the magnetization is tilted in plane [Fig. 3(c)].

Next, we analyze the SOT amplitudes normalized by the applied electric field  $B^{DL,FL}/E$ , shown in Figs. 4(a)–4(c). The motivation for this analysis is that the resistivity of Pd is strongly thickness dependent, as shown in Fig. 1(b). Therefore, even within a single sample, the current is not homogeneously distributed across the Pd layer. Moreover, the current profile in Pd can vary from sample to sample in a way that is not described by a simple parallel-resistor model. The electric field  $E = \rho j = \rho_{Pd} j_{Pd}$ , on the other hand, is the primary force driving the charge and spin currents [9] and is constant throughout the thickness of the whole sample, which makes it a practical unit for thickness-dependent studies of SOT [15,42]. Accordingly, in analogy

with Eq. (5) and for the purpose of comparing the SOT in different systems, we define the SOT efficiency per unit electric field [42]

$$\xi_E^{DL(FL)} = \frac{2e}{\hbar} M_s t_{Co} \frac{B^{DL(FL)}}{E} = \frac{\xi_j^{DL(FL)}}{\rho_{Pd}}. \quad (6)$$

Figure 4(a) shows that the thickness dependence of the electric-field-normalized SOT is very different from that of the current-normalized SOT:  $B_0^{DL}/E$  increases in an almost linear way in the whole range of  $t_{Pd}$ , while  $B_0^{FL}/E$  has a monotonic dependence on  $t_{Pd}$  and extrapolates to a nonzero value at  $t_{Pd} = 0$ . The angular amplitudes  $B_{2+4}^{DL}/E$ , on the other hand, are very small relative to  $B_0^{DL}/E$  and only weakly thickness dependent, contrary to the FL components  $B_{2+4}^{FL}/E$ , which have a strong dependence on  $t_{Pd}$ , as shown in Fig. 4(b). The implications of these results are discussed below.

### C. Discussion of spin-orbit torque dependence on Pd thickness

We discuss first the thickness dependence of the isotropic DL torque  $B_0^{DL}/j_{Pd}$  in terms of the drift-diffusion approach widely employed in the analysis of SOT and spin-pumping experiments. Assuming that the spin current flowing from the NM into the FM is uniquely due to the bulk SHE of the NM and is entirely absorbed at the NM-FM boundary [12], the simplest drift-diffusion model gives a dependence of the type  $\xi_j^{DL} = \gamma_{SH}[1 - \text{sech}(t_{Pd}/\lambda)]$ . A fit according to this function [gray line in Fig. 3(a)] yields  $\gamma_{SH} = 0.03$  and  $\lambda = 2$  nm, with an uncertainty of about 10%.

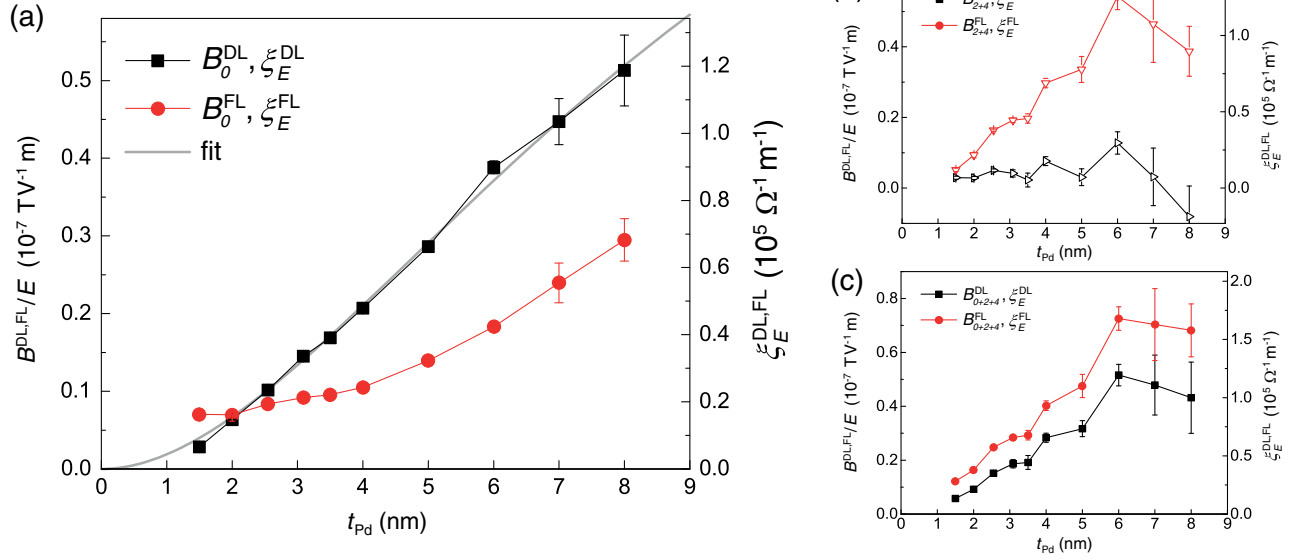


FIG. 4. SOT fields per unit electric field as a function of  $t_{\text{Pd}}$ . (a) Isotropic amplitudes  $B_0^{\text{DL}}/E$  and  $B_0^{\text{FL}}/E$ , corresponding to perpendicular magnetization. (b) Angle-dependent amplitudes  $B_{2+4}^{\text{DL}}/E$  and  $B_{2+4}^{\text{FL}}/E$ . (c) Total amplitudes for in-plane magnetization,  $B_{0+2+4}^{\text{DL}}/E$  and  $B_{0+2+4}^{\text{FL}}/E$ . The SOT efficiency  $\xi_E^{\text{DL(FL)}}$  is shown on the right scale.

There are, however, several reasons that caution against drawing conclusions from such a simplified model. First, within drift-diffusion theory, one should take into account the spin backflow into the NM [8,43] and spin-memory loss at the NM/FM interface [44,45]. Second, as pointed out in Ref. [42], drift-diffusion models assume constant  $\rho_{\text{NM}}$ ,  $\gamma_{\text{SH}}$ , and  $\lambda$  throughout the NM layer, whereas the strong dependence of  $\rho_{\text{NM}}$  on  $t_{\text{NM}}$  typical of ultrathin films [Fig. 1(b)] invalidates this hypothesis. Third, both first-principles electronic calculations [10,11] and optical measurements [46] suggest the existence of an “interface SHE,” which can be significantly larger than the bulk SHE. This interface SHE is ascribed to the current carried by interface states, similar to the Rashba-Edelstein effect [47]. Additionally, spin-dependent scattering at the FM/NM interface can also lead to a spin-polarized current and generate DL and FL SOTs [48,49]. Keeping track of all of these effects together leads to an overparametrized problem, which makes it difficult to draw a firm conclusion on either  $\gamma_{\text{SH}}$  or  $\lambda$ .

An alternative approach is to consider the SOT values normalized by the applied electric field. According to drift-diffusion theory and including spin backflow [8], the SOT efficiency per unit electric field due to the bulk SHE is given by

$$\xi_E^{\text{DL}} = 4\lambda \frac{\gamma_{\text{SH}}}{\rho} \sinh^2\left(\frac{t}{2\lambda}\right) \times \frac{2\lambda G_i^2 \cosh\left(\frac{t}{\lambda}\right) + G_r [2\lambda G_r \cosh\left(\frac{t}{\lambda}\right) + \frac{1}{\rho} \sinh\left(\frac{t}{\lambda}\right)]}{[2G_i \lambda \cosh\left(\frac{t}{\lambda}\right)]^2 + [2\lambda G_r \cosh\left(\frac{t}{\lambda}\right) + \frac{1}{\rho} \sinh\left(\frac{t}{\lambda}\right)]^2}, \quad (7)$$

$$\xi_E^{\text{FL}} = 4\lambda \frac{\gamma_{\text{SH}}}{\rho} \sinh^2\left(\frac{t}{2\lambda}\right) \times \frac{\frac{1}{\rho} G_i \sinh\left(\frac{t}{\lambda}\right)}{[2G_i \lambda \cosh\left(\frac{t}{\lambda}\right)]^2 + [2\lambda G_r \cosh\left(\frac{t}{\lambda}\right) + \frac{1}{\rho} \sinh\left(\frac{t}{\lambda}\right)]^2}, \quad (8)$$

where  $\rho$  and  $t$  are the resistivity and thickness of the normal-metal layer (Pd, in our case), while  $G_r$  and  $G_i$  are the real and imaginary parts of the spin-mixing conductance. The gray line in Fig. 3(c) is a fit to  $B_0^{\text{DL}}/E$  according to Eq. (7), which gives a spin Hall conductivity  $\sigma_{\text{SH}} = \gamma_{\text{SH}}/\rho = (4 \pm 1) \times 10^5 \Omega^{-1} \text{ m}^{-1}$  and  $\lambda = (7 \pm 1) \text{ nm}$ , assuming  $\rho_{\text{Pd}}^\infty = 1.4 \times 10^9 \Omega \text{ m}$  for the bulk Pd resistivity (measured for a 30-nm-thick Pd film), and the spin-mixing conductance calculated for a permalloy/Pd interface,  $G_r = 7.75 \times 10^{14} \Omega^{-1} \text{ m}^{-2}$  and  $G_i = G_r/7$  [50]. Although  $\lambda = 7 \text{ nm}$  is in good agreement with recent first-principles calculations of Pd [51],  $\sigma_{\text{SH}}$  exceeds the intrinsic value of  $2.1 \times 10^5 \Omega^{-1} \text{ m}^{-1}$  calculated for bulk Pd [50], and  $\gamma_{\text{SH}} = \rho_{\text{Pd}}^\infty \sigma_{\text{SH}} \approx 0.055$  is consistently larger than previously reported for Pd/permalloy bilayers in spin-pumping experiments [20–24,44,50]. An even larger estimate of  $\sigma_{\text{SH}}$  is obtained if we use  $G_r$  to  $5.94 \times 10^{14}$  calculated for a Co/Pt interface [8]. This analysis suggests that extrinsic or interface-related effects may enhance the DL SOT in Pd/Co/AIO<sub>x</sub> relative to what is expected from the bare SHE of Pd. The amplitude of the DL SOT, however, remains smaller than reported for Pt/Co/AIO<sub>x</sub> [14] and Pt/Co/MgO [42]. We remark that the observed variation of the torques cannot be related to changes of the film

roughness [52], which is approximately constant across the whole Pd/Co/ $\text{AlO}_x$  series. We also note that a refinement of the drift-diffusion model that considers a thickness-dependent  $\lambda$  rescaled such that the product  $\rho_{\text{Pd}}\lambda$  is constant and equal to the bulk value  $\rho_{\text{Pd}}^\infty\lambda^\infty$ , consistent with the Elliott-Yafet mechanism of spin relaxation [42], gives  $\sigma_{\text{SH}} = (5 \pm 2) \times 10^5 \Omega^{-1} \text{ m}^{-1}$  and  $\lambda = (18 \pm 8) \text{ nm}$ , showing that the fitted values of  $\sigma_{\text{SH}}$  and  $\lambda$  are strongly model dependent. Even such a refined model, however, does not take into account the interface enhancement of the SHE [10,11,48,49] and cannot justify the presence of a large FL SOT.

A similar analysis can be performed on  $B_{0+2+4}^{\text{DL}}$ , corresponding to the SOT efficiency for the in-plane magnetization [Fig. 3(c)]; the main result in this case is a reduction of  $\lambda$  by 20%–40% relative to the out-of-plane case discussed above. Such a result is not so surprising if one considers that spin diffusion in the limit of  $t_{\text{Pd}} \geq \lambda$  is strongly influenced by the NM/FM interface, where spin-orbit coupling is responsible for inducing anisotropic electron scattering processes. For the same reason, one may expect also the spin-mixing conductance and spin-memory loss to depend on the magnetization direction.

We now discuss the thickness dependence of the FL SOT, which is qualitatively different than the DL SOT. The  $B_0^{\text{FL}}/j_{\text{Pd}}$  ratio [full dots in Fig. 3(a)] has a nonmonotonic behavior as a function of  $t_{\text{Pd}}$ , with a minimum around 3.5 nm. This behavior compounds the FL SOT thickness dependence with the uneven current distribution in the Pd/Co bilayer. Analyzing the ratio  $B_0^{\text{FL}}/E$  [full dots in Fig. 4(a)] obviates the problem of the current distribution, revealing a monotonic increase of  $B_0^{\text{FL}}/E$  with an increasing  $t_{\text{Pd}}$ . Unlike  $B_0^{\text{DL}}/E$ , however,  $B_0^{\text{FL}}/E$  extrapolates to a nonzero value at  $t_{\text{Pd}} = 0$ , evidencing a significant contribution from the Pd/Co interface akin to a Rashba-Edelstein magnetic field [41,53]. Moreover, an attempt to fit  $\xi_E^{\text{FL}}$  using the SHE drift-diffusion theory [Eq. (8)] adding a constant term for the interface contribution yields a  $\sigma_{\text{SH}}$  about one order of magnitude larger than that derived from the analysis of  $\xi_E^{\text{DL}}$ . Similar considerations apply to  $B_{0+2+4}^{\text{FL}}$ . The comparison between  $B_{2+4}^{\text{FL}}$  and  $B_{2+4}^{\text{DL}}$  in Fig. 4(b) further shows that the FL torque has a stronger anisotropic component relative to the DL torque, and that such anisotropy is thickness dependent. This finding is in contrast to the standard form of the SOTs derived from the bulk SHE using either the drift-diffusion model or the Boltzmann transport equation, exemplified by Eqs. (7) and (8), which predict only the existence of the isotropic terms  $B_0^{\text{DL}}$  and  $B_0^{\text{FL}}$  [8]. Although there is presently no theory providing a complete description of the torque anisotropy in realistic FM-HM systems including both bulk and interfacial spin-orbit coupling, a possible explanation is that the angular dependence of the torques arises from anisotropic spin-dependent scattering at the FM/HM

interface or inside the FM, which affects the amplitude of the nonequilibrium spin currents in the bilayer.

The observation of a thickness-independent FL SOT and of strongly enhanced DL and FL amplitudes relative to those expected from the bulk SHE of Pd leads to the conclusion that interface effects contribute significantly to the current-induced SOTs in Pd/Co/ $\text{AlO}_x$ . Such effects are ubiquitous, but they may be particularly evident in Pd because of the reduced bulk SHE compared to 5d-metal systems. The standard drift-diffusion theory of the SHE [8,43], which is routinely used to extract  $\gamma_{\text{SH}}$  and  $\lambda$  from spin-pumping and SOT measurements, does not account for interface terms, thickness-dependent spin-diffusion parameters, or angle-dependent SOT.

Similarly, two-dimensional models of the Rashba-Edelstein effect do not properly describe the spin-accumulation profile in FM/HM layers and neglect the bulk SHE of the HM [53]. More recent theoretical work consequently points out the need to include the bulk- and interface-generated spin accumulation on the same footing in three-dimensional models of electron transport [48,49]. A key prediction of the latter work is that interfacial spin-orbit scattering creates substantial spin currents that flow away from the FM/HM interface, generating both DL and FL torques. The thickness dependence of the two torques differs, with the interfacial FL torque being nearly thickness independent and the interfacial DL torque increasing with the thickness of the NM layer [49]. This finding is qualitatively consistent with the results reported in Fig. 4, namely, a FL torque comprising a thickness-independent term and a DL torque that is strongly thickness dependent. In this scenario, both torques would include bulk and interface contributions of comparable magnitude. Another prediction of this theory is that the interfacial scattering amplitudes depend on the magnetization direction, which naturally leads to anisotropic SOT as well as magnetoresistance [48,49].

In this respect, it is interesting to draw a parallel between the angular dependence of the SOT and magnetoresistance in metallic FM/HM bilayers. Figures 3 and 4 show that the SOT amplitude increases strongly when  $\mathbf{m}$  is tilted towards the  $y$  direction and only moderately when  $\mathbf{m}$  is tilted towards the  $x$  direction. This behavior is similar to that of the magnetoresistance in FM/HM layers, which shows much greater change when  $\mathbf{m}$  is rotated in the  $y$ - $z$  plane relative to rotations in the  $x$ - $z$  plane [54,55]. Exploring this connection goes beyond the scope of this work, but we believe that additional studies of the correlation between SOT and anisotropic magnetoresistance [19] may help us to understand transport at interfaces with spin-orbit coupling.

#### D. Magnetization switching

Finally, we address the question of whether the SOTs provided by Pd are sufficient to reverse the magnetization of the Co layer in a controlled way. To our knowledge,

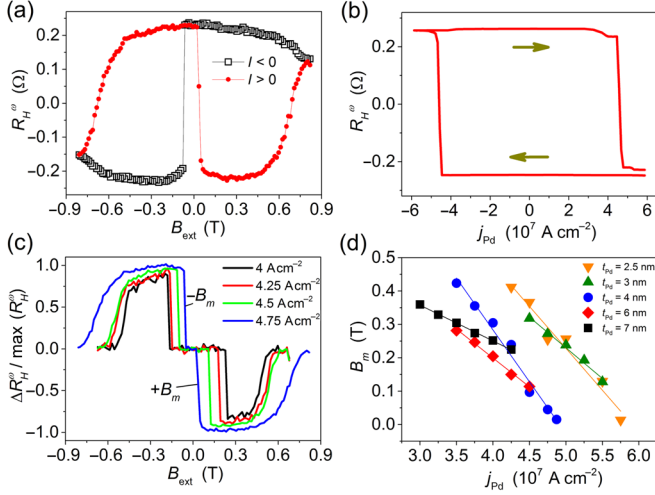


FIG. 5. (a) Change of the Hall resistance due to magnetization switching induced by positive and negative current pulses with amplitude  $j_{\text{Pd}} = 4.75 \text{ A/cm}^2$  ( $I = 11 \text{ mA}$ ) as a function of the external field  $B_{\text{ext}}$  in Pd(4 nm)/Co(0.6 nm)/AlO<sub>x</sub>. The external field is applied in-plane parallel to the current direction ( $\theta_B = 89.7^\circ$ ,  $\varphi = 0^\circ$ ). (b) Hall resistance as a function of  $j_{\text{Pd}}$  at a constant  $B_{\text{ext}} = 0.2 \text{ T}$ . (c) Normalized difference of the Hall resistance measured for  $I > 0$  and  $I < 0$  in (a) as a function of  $B_{\text{ext}}$ . Similar curves are shown also for different values of  $j_{\text{Pd}}$ . (d) Minimum switching field  $B_m$  as a function of  $j_{\text{Pd}}$  and  $t_{\text{Pd}}$ .

SOT-driven switching using 4d-metal layers has not yet been reported. Figure 5(a) shows the results of a typical switching experiment, performed by injecting 0.3 s long current pulses of positive and negative polarity in a Pd(4 nm)/Co(0.6 nm)/AlO<sub>x</sub> Hall bar. The plot shows the change of the Hall resistance after each pulse due to switching of the magnetization from up to down and vice versa during a single sweep of the in-plane external field, from  $-0.82$  to  $0.82 \text{ T}$ .

An alternative demonstration of current-induced switching is reported in Fig. 5(b), where the Hall resistance is recorded as a function of current for a constant in-plane field. As discussed in previous work [1,2], the purpose of the in-plane field is to break the symmetry of the DL SOT and univocally determine the switching direction, which occurs through the expansion of chiral domain walls [6]. Figure 5(c) shows the difference of the Hall resistance  $\Delta R_H^o$  measured after two consecutive current pulses, one positive and one negative, normalized to its saturation value. Switching is obtained whenever  $|\Delta R_H^o| > 0$ .

We observe that the minimum field required to achieve deterministic switching,  $B_m$ , decreases linearly with an increasing current, as shown in Fig. 5(d), similar to Pt/Co/AlO<sub>x</sub> [1] and Ta/CoFeB/MgO [16]. Such a linear behavior is found in all samples, albeit with a different slope, which we attribute to differences in the domain nucleation field. The minimum current density required to achieve deterministic switching depends on  $t_{\text{Pd}}$  and is generally smaller in the thicker samples, as expected due

to the overall increase of the SOT with an increasing  $t_{\text{Pd}}$  (Fig. 3). Remarkably, the dc current density required to switch Pd/Co/AlO<sub>x</sub> is similar (within a factor of 2) to that used to switch Pt/Co/MgO and Pt/Co/AlO<sub>x</sub> dots with comparable PMA [2,5], which is in agreement with the relatively large SOT efficiency reported in this work.

#### IV. CONCLUSIONS

We performed magnetotransport, magnetic-anisotropy, and SOT vector measurements of Pd/Co(0.6 nm)/AlO<sub>x</sub> layers as a function of Pd thickness. We found that the PMA of Pd/Co is reinforced by optimum oxidation of the Al capping layer relative to Pd/Co multilayers, yielding a magnetic anisotropy energy of  $(1.5 \pm 0.1) \times 10^6 \text{ J/m}^3$ , which is nearly independent of  $t_{\text{Pd}}$ . Current injection in Pd/Co/AlO<sub>x</sub> leads to sizable DL and FL SOTs that have the same order of magnitude, about 1 mT per  $10^7 \text{ A/cm}^2$ , but different thicknesses and angular dependence.

The analysis of the DL SOT yields a relatively large effective spin Hall angle for Pd,  $\gamma_{\text{SH}} \approx 0.03\text{--}0.06$ , or a spin Hall conductivity  $\sigma_{\text{SH}} = (4 \pm 1) \times 10^5 \text{ } \Omega^{-1} \text{ m}^{-1}$ , depending on the model used to fit the data. The DL spin-torque efficiency per unit electric field is on the order of  $10^5 \text{ } \Omega^{-1} \text{ m}^{-1}$ , only a factor of 2 smaller relative to Pt/Co/MgO layers of comparable thickness [42].  $\gamma_{\text{SH}}$  is enhanced compared to Pd/permalloy bilayers [20–24], but it is significantly smaller than that reported for [Pd/Co]<sub>N</sub> multilayers [25] and Pd/FePd/MgO [26].

Additionally, our data evidence a strong FL SOT, with an interface contribution that extrapolates to a finite value at  $t_{\text{Pd}} = 0$ , and up to a threefold enhancement of the FL SOT efficiency when the magnetization rotates from the out-of-plane to the in-plane direction transverse to the current. Overall, our results indicate that SOT models based on one-dimensional drift-diffusion theory and a bulk SHE do not adequately capture the SOT dependence on Pd thickness, at least based on a single set of  $\sigma_{\text{SH}}$ ,  $\lambda$ ,  $G_r$ , and  $G_i$  parameters. A possible scenario is that spin currents driven by interfacial spin-orbit scattering add up to the spin currents induced by the bulk SHE of Pd [49], resulting in the nontrivial thickness and angle dependence of the SOT observed here.

Finally, we report bipolar magnetization switching in Pd/Co/AlO<sub>x</sub> for  $j_{\text{Pd}} = 3\text{--}6 \times 10^7 \text{ A/cm}^2$ , depending on the Pd thickness and in-plane applied field. These results show that Pd/Co/oxide layers with relatively low resistivity can be used to combine strong PMA with efficient current-induced magnetization switching, opening the possibility of using Pd as an alternative material to Pt, Ta, and W in SOT devices.

#### ACKNOWLEDGMENTS

This work was supported by the Swiss National Science Foundation (Grant No. 200021-153404) and the European

Commission under the Seventh Framework Program (spOt project, Grant No. 318144). We thank Junxiao Feng and Luca Persichetti for performing the roughness measurements.

- 
- [1] I. M. Miron, K. Garello, G. Gaudin, P.-J. Zermatten, M. V. Costache, S. Auffret, S. Bandiera, B. Rodmacq, A. Schuhl, and P. Gambardella, Perpendicular switching of a single ferromagnetic layer induced by in-plane current injection, *Nature (London)* **476**, 189 (2011).
- [2] C. O. Avci, K. Garello, I. M. Miron, G. Gaudin, S. Auffret, O. Boulle, and P. Gambardella, Magnetization switching of an MgO/Co/Pt layer by in-plane current injection, *Appl. Phys. Lett.* **100**, 212404 (2012).
- [3] L. Liu, C.-F. Pai, Y. Li, H. W. Tseng, D. C. Ralph, and R. A. Buhrman, Spin-torque switching with the giant spin Hall effect of tantalum, *Science* **336**, 555 (2012).
- [4] M. Cubukcu, O. Boulle, M. Drouard, K. Garello, C. O. Avci, I. M. Miron, J. Langer, B. Ocker, P. Gambardella, and G. Gaudin, Spin-orbit torque magnetization switching of a three-terminal perpendicular magnetic tunnel junction, *Appl. Phys. Lett.* **104**, 042406 (2014).
- [5] K. Garello, C. O. Avci, I. M. Miron, M. Baumgartner, A. Ghosh, S. Auffret, O. Boulle, G. Gaudin, and P. Gambardella, Ultrafast magnetization switching by spin-orbit torques, *Appl. Phys. Lett.* **105**, 212402 (2014).
- [6] N. Perez, E. Martinez, L. Torres, S.-H. Woo, S. Emori, and G. S. D. Beach, Chiral magnetization textures stabilized by the Dzyaloshinskii-Moriya interaction during spin-orbit torque switching, *Appl. Phys. Lett.* **104**, 092403 (2014).
- [7] C. Zhang, S. Fukami, H. Sato, F. Matsukura, and H. Ohno, Spin-orbit torque induced magnetization switching in nanoscale Ta/CoFeB/MgO, *Appl. Phys. Lett.* **107**, 012401 (2015).
- [8] P. M. Haney, H.-W. Lee, K.-J. Lee, A. Manchon, and M. D. Stiles, Current induced torques and interfacial spin-orbit coupling: Semiclassical modeling, *Phys. Rev. B* **87**, 174411 (2013).
- [9] F. Freimuth, S. Blügel, and Y. Mokrousov, Spin-orbit torques in Co/Pt (111) and Mn/W (001) magnetic bilayers from first principles, *Phys. Rev. B* **90**, 174423 (2014).
- [10] F. Freimuth, S. Blügel, and Y. Mokrousov, Direct and inverse spin-orbit torques, *Phys. Rev. B* **92**, 064415 (2015).
- [11] L. Wang, R. J. H. Wesselink, Y. Liu, Z. Yuan, K. Xia, and P. J. Kelly, Giant Room Temperature Interface Spin Hall and Inverse Spin Hall Effects, *Phys. Rev. Lett.* **116**, 196602 (2016).
- [12] L. Liu, T. Moriyama, D. C. Ralph, and R. A. Buhrman, Spin-Torque Ferromagnetic Resonance Induced by the Spin Hall Effect, *Phys. Rev. Lett.* **106**, 036601 (2011).
- [13] C.-F. Pai, L. Liu, Y. Li, H. W. Tseng, D. C. Ralph, and R. A. Buhrman, Spin transfer torque devices utilizing the giant spin Hall effect of tungsten, *Appl. Phys. Lett.* **101**, 122404 (2012).
- [14] K. Garello, I. M. Miron, C. O. Avci, F. Freimuth, Y. Mokrousov, S. Blügel, S. Auffret, O. Boulle, G. Gaudin, and P. Gambardella, Symmetry and magnitude of spin-orbit torques in ferromagnetic heterostructures, *Nat. Nanotechnol.* **8**, 587 (2013).
- [15] J. Kim, J. Sinha, M. Hayashi, M. Yamanouchi, S. Fukami, T. Suzuki, S. Mitani, and H. Ohno, Layer thickness dependence of the current-induced effective field vector in Ta|CoFeB|MgO, *Nat. Mater.* **12**, 240 (2013).
- [16] C. O. Avci, K. Garello, C. Nistor, S. Godey, B. Ballesteros, A. Mugarza, A. Barla, M. Valvidares, E. Pellegrin, A. Ghosh, I. M. Miron, O. Boulle, S. Auffret, G. Gaudin, and P. Gambardella, Fieldlike and antidamping spin-orbit torques in as-grown and annealed Ta/CoFeB/MgO layers, *Phys. Rev. B* **89**, 214419 (2014).
- [17] X. Fan, H. Celik, J. Wu, C. Ni, K.-J. Lee, V. O. Lorenz, and J. Q. Xiao, Quantifying interface and bulk contributions to spin-orbit torque in magnetic bilayers, *Nat. Commun.* **5**, 3042 (2014).
- [18] J. Torrejon, J. Kim, J. Sinha, S. Mitani, M. Hayashi, M. Yamanouchi, and H. Ohno, Interface control of the magnetic chirality in CoFeB/MgO heterostructures with heavy-metal underlayers, *Nat. Commun.* **5**, 4655 (2014).
- [19] C. O. Avci, K. Garello, J. Mendil, A. Ghosh, N. Blasakis, M. Gabureac, M. Trassin, M. Fiebig, and P. Gambardella, Magnetoresistance of heavy and light metal/ferromagnet bilayers, *Appl. Phys. Lett.* **107**, 192405 (2015).
- [20] M. Morota, Y. Niimi, K. Ohnishi, D. H. Wei, T. Tanaka, H. Kontani, T. Kimura, and Y. Otani, Indication of intrinsic spin Hall effect in 4d and 5d transition metals, *Phys. Rev. B* **83**, 174405 (2011).
- [21] K. Kondou, H. Sukegawa, S. Mitani, K. Tsukagoshi, and S. Kasai, Evaluation of spin Hall angle and spin diffusion length by using spin current-induced ferromagnetic resonance, *Appl. Phys. Express* **5**, 073002 (2012).
- [22] Z. Tang, Y. Kitamura, E. Shikoh, Y. Ando, T. Shinjo, and M. Shiraishi, Temperature dependence of spin Hall angle of palladium, *Appl. Phys. Express* **6**, 083001 (2013).
- [23] V. Vlaminc, J. E. Pearson, S. D. Bader, and A. Hoffmann, Dependence of spin-pumping spin Hall effect measurements on layer thicknesses and stacking order, *Phys. Rev. B* **88**, 064414 (2013).
- [24] C. T. Boone, H. T. Nembach, J. M. Shaw, and T. J. Silva, Spin transport parameters in metallic multilayers determined by ferromagnetic resonance measurements of spin-pumping, *J. Appl. Phys.* **113**, 153906 (2013).
- [25] M. Jamali, K. Narayanapillai, X. Qiu, L. Ming Loong, A. Manchon, and H. Yang, Spin-Orbit Torques in Co/Pd Multilayer Nanowires, *Phys. Rev. Lett.* **111**, 246602 (2013).
- [26] H.-R. Lee, K. Lee, J. Cho, Y.-H. Choi, C.-Y. You, M.-H. Jung, F. Bonell, Y. Shiota, S. Miwa, and Y. Suzuki, Spin-orbit torque in a bulk perpendicular magnetic anisotropy Pd/FePd/MgO system, *Sci. Rep.* **4**, 6548 (2014).
- [27] U. Hwan Pi, K. Won Kim, J. Young Bae, S. Chul Lee, Y. Jin Cho, K. Seok Kim, and S. Seo, Tilting of the spin orientation induced by Rashba effect in ferromagnetic metal layer, *Appl. Phys. Lett.* **97**, 162507 (2010).
- [28] M. Hayashi, J. Kim, M. Yamanouchi, and H. Ohno, Quantitative characterization of the spin-orbit torque using harmonic Hall voltage measurements, *Phys. Rev. B* **89**, 144425 (2014).
- [29] C. O. Avci, K. Garello, M. Gabureac, A. Ghosh, A. Fuhrer, S. F. Alvarado, and P. Gambardella, Interplay of spin-orbit



- torque and thermoelectric effects in ferromagnet/normal-metal bilayers, *Phys. Rev. B* **90**, 224427 (2014).
- [30] See Supplemental Material at <http://link.aps.org/supplemental/10.1103/PhysRevApplied.7.014004> for showing the separation of the thermal and spin-orbit torque contributions to the second harmonic hall resistance.
- [31] X. Qiu, P. Deorani, K. Narayanapillai, K.-S. Lee, K.-J. Lee, H.-W. Lee, and H. Yang, Angular and temperature dependence of current induced spin-orbit effective fields in Ta/CoFeB/MgO nanowires, *Sci. Rep.* **4**, 4491 (2014).
- [32] K.-S. Lee, D. Go, A. Manchon, P. M. Haney, M. D. Stiles, H.-W. Lee, and K.-J. Lee, Angular dependence of spin-orbit spin-transfer torques, *Phys. Rev. B* **91**, 144401 (2015).
- [33] S. M. Shivaprasad, L. A. Udachan, and M. A. Angadi, Electrical resistivity of thin palladium films, *Phys. Lett.* **78A**, 187 (1980).
- [34] G. Fischer, H. Hoffmann, and J. Vancea, Mean free path and density of conductance electrons in platinum determined by the size effect in extremely thin films, *Phys. Rev. B* **22**, 6065 (1980).
- [35] Z. B. Guo, W. B. Mi, R. O. Aboljadayel, B. Zhang, Q. Zhang, P. G. Barba, A. Manchon, and X. X. Zhang, Effects of surface and interface scattering on anomalous Hall effect in Co/Pd multilayers, *Phys. Rev. B* **86**, 104433 (2012).
- [36] P. F. Carcia, A. D. Meinhardt, and A. Suna, Perpendicular magnetic anisotropy in Pd/Co thin film layered structures, *Appl. Phys. Lett.* **47**, 178 (1985).
- [37] O. Hellwig, T. Hauet, T. Thomson, E. Dobisz, J. D. Risner-Jamtegaard, D. Yaney, B. D. Terris, and E. E. Fullerton, Coercivity tuning in Co/Pd multilayer based bit patterned media, *Appl. Phys. Lett.* **95**, 232505 (2009).
- [38] K. Yakushiji, T. Saruya, H. Kubota, A. Fukushima, T. Nagahama, S. Yuasa, and K. Ando, Ultrathin Co/Pt and Co/Pd superlattice films for MgO-based perpendicular magnetic tunnel junctions, *Appl. Phys. Lett.* **97**, 232508 (2010).
- [39] H. X. Yang, M. Chshiev, B. Dieny, J. H. Lee, A. Manchon, and K. H. Shin, First-principles investigation of the very large perpendicular magnetic anisotropy at Fe|MgO and Co|MgO interfaces, *Phys. Rev. B* **84**, 054401 (2011).
- [40] I. G. Rau, S. Baumann, S. Rusponi, F. Donati, S. Stepanow, L. Gragnaniello, J. Dreiser, C. Piamonteze, F. Nolting, S. Gangopadhyay *et al.*, Reaching the magnetic anisotropy limit of a 3d metal atom, *Science* **344**, 988 (2014).
- [41] I. M. Miron, G. Gaudin, S. Auffret, B. Rodmacq, A. Schuhl, S. Pizzini, J. Vogel, and P. Gambardella, Current-driven spin torque induced by the Rashba effect in a ferromagnetic metal layer, *Nat. Mater.* **9**, 230 (2010).
- [42] M.-H. Nguyen, D. C. Ralph, and R. A. Buhrman, Spin Torque Study of the Spin Hall Conductivity and Spin Diffusion Length in Platinum Thin Films with Varying Resistivity, *Phys. Rev. Lett.* **116**, 126601 (2016).
- [43] Y.-T. Chen, S. Takahashi, H. Nakayama, M. Althammer, S. T. B. Goennenwein, E. Saitoh, and G. E. W. Bauer, Theory of spin Hall magnetoresistance, *Phys. Rev. B* **87**, 144411 (2013).
- [44] H. Kurt, R. Loloee, K. Eid, W. P. Pratt, and J. Bass, Spin-memory loss at 4.2 K in sputtered Pd and Pt and at Pd/Cu and Pt/Cu interfaces, *Appl. Phys. Lett.* **81**, 4787 (2002).
- [45] J.-C. Rojas-Sánchez, N. Reyren, P. Laczkowski, W. Saverio, J.-P. Attané, C. Deranlot, M. Jamet, J.-M. George, L. Vila, and H. Jaffrès, Spin Pumping and Inverse Spin Hall Effect in Platinum: The Essential Role of Spin-Memory Loss at Metallic Interfaces, *Phys. Rev. Lett.* **112**, 106602 (2014).
- [46] F. Bottegoni, A. Ferrari, F. Rortais, C. Vergnaud, A. Marty, G. Isella, M. Finazzi, M. Jamet, and F. Ciccacci, Spin diffusion in Pt as probed by optically generated spin currents, *Phys. Rev. B* **92**, 214403 (2015).
- [47] J. C. Rojas Sánchez, L. Vila, G. Desfonds, S. Gambarelli, J. P. Attané, J. M. De Teresa, C. Magén, and A. Fert, Spin-to-charge conversion using Rashba coupling at the interface between non-magnetic materials, *Nat. Commun.* **4**, 2944 (2013).
- [48] V. P. Amin and M. D. Stiles, Spin transport at interfaces with spin-orbit coupling: Formalism, *Phys. Rev. B* **94**, 104419 (2016).
- [49] V. P. Amin and M. D. Stiles, Spin transport at interfaces with spin-orbit coupling: Phenomenology, *Phys. Rev. B* **94**, 104420 (2016).
- [50] W. Zhang, M. B. Jungfleisch, W. Jiang, Y. Liu, J. E. Pearson, S. G. E. te Velthuis, A. Hoffmann, F. Freimuth, and Y. Mokrousov, Reduced spin-Hall effects from magnetic proximity, *Phys. Rev. B* **91**, 115316 (2015).
- [51] Y. Liu, Z. Yuan, R. J. H. Wesselink, A. A. Starikov, M. van Schilfgaarde, and P. J. Kelly, Direct method for calculating temperature-dependent transport properties, *Phys. Rev. B* **91**, 220405 (2015).
- [52] L. Zhou, V. L. Grigoryan, S. Maekawa, X. Wang, and J. Xiao, Spin Hall effect by surface roughness, *Phys. Rev. B* **91**, 045407 (2015).
- [53] A. Manchon and S. Zhang, Theory of nonequilibrium intrinsic spin torque in a single nanomagnet, *Phys. Rev. B* **78**, 212405 (2008).
- [54] A. Kobs, S. Heße, W. Kreuzpaintner, G. Winkler, D. Lott, P. Weinberger, A. Schreyer, and H. P. Oepen, Anisotropic Interface Magnetoresistance in Pt/Co/Pt Sandwiches, *Phys. Rev. Lett.* **106**, 217207 (2011).
- [55] C. O. Avci, K. Garello, A. Ghosh, M. Gabureac, S. F. Alvarado, and P. Gambardella, Unidirectional spin Hall magnetoresistance in ferromagnet/normal metal bilayers, *Nat. Phys.* **11**, 570 (2015).